Vesicles of Toroidal Topology: Observed Morphology and Shape Transformations

Xavier Michalet, David Bensimon

J. Phys. II France **5** (1995) 263–287 FEBRUARY **1995**, PAGE 263

Classification
Physics Abstracts
82.70 — 02.40 — 68.15

Vesicles of Toroidal Topology: Observed Morphology and Shape Transformations

Xavier Michalet and David Bensimon

Laboratoire de Physique Statistique, Ecole Normale Supérieure, 24 rue Lhomond, 75231 Paris Cedex 5, France

(Received 9 August 1994, received in final form, accepted 24 October 1994)

Résumé. — Nous présentons des observations de vésicules toroïdales de sections méridiennes circulaires et non circulaires, axisymétriques et non axisymétriques. Nous décrivons également des modifications de forme dues à des changements de température, qui permettent de faire le lien avec une conjecture mathématique due à Willmore. Nos observations sont analysées à l'aide d'une procédure numérique qui permet de déterminer les paramètres géométriques pertinents des formes des vésicules. Une comparaison de nos observations avec des prédictions théoriques récentes est faite, qui permet de mettre en évidence certaines caractéristiques imprévues des formes d'équilibre observées.

Abstract. — We report observations of toroidal vesicles with circular and noncircular cross sections, axisymmetric and nonaxisymmetric. Shape transformations induced by temperature changes are also described, which permit a connection to a mathematical conjecture due to Willmore. Our observations are analysed using a numerical procedure which allows a determination of the relevant geometrical parameters of the shapes. We compare these observations with recent theoretical predictions and point out some unexpected properties of the observed equilibrium shapes.

1. Introduction

1.1. The Physics of Closed Fluid Bilayers. — Study of the equilibrium shape of artificial vesicles has been developed both theoretically and experimentally in different groups during the past 20 years [1–3] (for an introductory review, see [4]). Vesicles are made of a closed fluid phospholipid bilayer (the membrane) whose thickness is of the order of twice the size of a phospholipid molecule (i.e., approximately 5 nm), their typical linear size (radius) being of the order of some tens of micrometers. They are very easily prepared, for example, by excess hydration of a dense lamellar phase (see experimental methods). Due to their thinness, vesicles are observed using phase contrast optical microscopy. They appear as dark closed lines, which represent approximately the apparent contour of the vesicle shapes perpendicular to the optical axis of the microscope.

The energetics of these objects is simple, due to the zero elastic shear modulus and incompressibility of the fluid membrane and to the absence of an effective surface tension. For these reasons, the bending elastic energy is the dominant term, and the approximately 2D surface has thus a *Curvature Elastic Energy* (CEE):

$$E_0 = \frac{\kappa}{2} \iint (2H)^2 \mathrm{d}S, \tag{1}$$

where $H = \frac{1}{2}\left(\frac{1}{R_1} + \frac{1}{R_2}\right)$ is the local mean curvature of the surface, R_1, R_2 being its radii of principal curvature, and $\kappa \approx 10 - 20 k_B T$ being the bending modulus of the membrane [5]. The determination of the possible mechanical equilibrium shapes consists then in a minimization of (1), under some additional physical constraints.

These constraints come from the physico-chemical characteristics of the membrane. The amphiphilic nature of the phospholipid molecules leads to a negligible exchange rate between the aqueous environment and the membrane, as well as between the two monolayers of the membrane. As a consequence, during a typical experiment, one can assume that the number of molecules is constant in both monolayers. Being incompressible, the area A of the vesicle is thus a constant, as well as the area asymmetry $\Delta A = A^{\mathrm{out}} - A^{\mathrm{in}}$ between the inner and outer monolayers. In addition, at mechanical equilibrium the osmotic pressure difference is zero between the inside and the ouside of the vesicle, resulting in no net water exchange across the membrane: the volume V of the vesicle is thus also a constant fixed at the time of equilibration.

1.2 Phenomenological Models — To take into account these three different constraints A, ΔA and V, one has to introduce three Lagrange parameters, λ, μ and p. The functional to be minimized is thus:

$$F_{\mathrm{BC}} = E_0 + \lambda A + pV + \mu \Delta A. \tag{2}$$

This model is known as the *Bilayer Coupling model* (BC), because it explicitly takes into account the bilayer nature of the membrane [6, 7].

Another approach has been proposed which describes the possible asymmetry of the bilayer in terms of a spontaneous curvature. Instead of (1), one writes:

$$E_{\mathrm{SC}} = \frac{\kappa}{2} \iint (2H - C_0)^2 \mathrm{d}S, \tag{3}$$

where $\frac{1}{2}C_0$ is the preferred local mean curvature of the membrane, which one can for example attribute *a posteriori* to the area asymmetry between the inner and outer monolayers, but also to different chemical compositions or environments of the inner and outer monolayers [8]. In this *Spontaneous Curvature model* (SC), the functional to be minimized is:

$$F_{\mathrm{SC}} = E_{\mathrm{SC}} + \lambda A + pV. \tag{4}$$

Finally, some authors have proposed to consider a more general model, which has the two preceding ones as limiting cases [9–11]. The *Area Difference Elasticity model* (ADE) sets an elastic cost on the deviation of the bilayer from its preferred area difference ΔA_0. Explicitly, one adds a term to (3) and gets for the elastic energy of the membrane:

$$E_{\mathrm{ADE}} = \frac{\kappa}{2} \iint (2H - C_0)^2 \mathrm{d}S + \alpha \frac{\kappa}{2} \left(\frac{1}{2DR_0}\right)^2 (\Delta A - \Delta A_0)^2. \tag{5}$$

The coefficient α is a phenomenological parameter of order 1,

$$R_0 = \sqrt{\frac{A}{4\pi}}, \tag{6}$$

and D is the thickness of the bilayer. For $\alpha \to 0$, one recovers the SC model, and for $\alpha \to \infty$, the BC model.

All these models lead to the same Euler-Lagrange equations and thus, the whole set of stationary solutions is the same in all three models. However, each model being characterized by a different curvature elastic energy, a stationary shape can be either a local minimum, a local maximum or a local saddle point, depending on the model considered. We will call a *stable shape* of a model a surface which is the solution of the Euler-Lagrange equations for a given set of geometrical parameters *and* is the absolute minimum of the energy (E_0 in the BC model, E_{SC} in the SC model, E_{ADE} in the ADE model); all other solutions (local minima of the energy) will be called *metastable shapes.*

1.3. Results and Experiments for Spherical Topology. — The equilibrium shapes of spherical topology (topological genus 0) have been calculated in both BC and SC models, leading to a phase diagram of the expected vesicles which depends on the imposed geometrical constraints [8, 12, 13]. At this point, one has to note that the CEE (1) being scale invariant, it is always possible to end up with a shape of the desired area by a simple rescaling. Therefore, only two geometrical constraints are relevant. For simplicity, one uses the following dimensionless ones:

- the reduced volume

$$v = 6\sqrt{\pi}V/A^{3/2}, \tag{7}$$

  which reaches its maximum value of 1 for the sphere,

- the reduced area difference,

$$\Delta a = \Delta A/(2R_0D) = \iint H\mathrm{d}S/(8\pi R_0 D), \tag{8}$$

- and/or the reduced spontaneous curvature

$$c_0 = C_0 R_0. \tag{9}$$

In conclusion, one can predict the stable equilibrium shape for any (v, c_0) in the SC model, for any $(v, \Delta a)$ in the BC model, and for any $(v, c_0, \Delta a_0)$ in the ADE model. For details on the results obtained in the genus 0 case, we refer the reader to the original articles.

By modeling the effects of a temperature change on the geometrical parameters of the vesicle, it is also possible to predict the behaviour of the shape of a vesicle subjected to such a progressive change. Different shape transformations have been observed and numerically calculated, among which the most famous is the so called "budding transition". The predicted order of the transition depending in some cases on the model (SC, BC or ADE), it is in principle possible to discriminate between them. This comparison between experiments and theories is satisfactory for equilibrium shapes, but the order of the observed shape transformations is still an open issue.

1.4. TOROIDAL TOPOLOGY. — Our purpose is to present new experimental results on vesicles of toroidal topology and to compare them with recent predictions. The paper is organized as follows: a first part (Sect. 2) describes the experimental methods. A summary of the theoretical predictions is given in Section 3. We describe in Section 4 our observations of toroidal vesicles with circular cross sections, both axisymmetric and nonaxisymmetric and we report results on shape transformations induced by temperature changes. In Section 5, we report the first observation of discoid nonaxisymmetric vesicles. Section 6 describes the first observed toroidal stomatocyte. Section 7 discusses possible experimental reasons for the nonobservation of sickle-shaped tori. We conclude this article with a summary of the theoretical implications of our experiments.

2. Experimental Methods

2.1. PREPARATION OF VESICLES. — Vesicles are made of one (or more) closed bilayers. They are mostly prepared with multicomponent mixtures of natural phospholipids swelled in water by using various procedures. They can also be prepared with very pure synthetic surfactants. We used pure synthetic "standard" phospholipids purchased from Avanti Polar Lipids, Inc. (DMPC, DPPC, DOPC) as well as a polymerizable one, $DC_{8,9}PC$ [14–16].

- For the first ones (DMPC, DPPC, DOPC), we used crystallized phospholipids (a few mg) deposited on a Petri dish. A droplet of de-ionized water (at a temperature $T > T_m$) swells the lipids which are then spread over the bottom of the box. A further excess amount of heated de-ionized water (some ml) permits the separation of vesicles from the bulk lamellar phase (complete swelling occurs after some hours). Vesicles of non spherical topological genus represent only a very small part of the overall population (much less than 1%).

- The last phospholipid ($DC_{8,9}PC$) can be swelled in a similar way. When cooled below the melting temperature of the chains ($T_m = 42$ °C), vesicles undergo a morphological transition toward tubules (diameter: 1 μm, length: some 100 μm) due to the chirality of the molecules. This transition is reversible, which means that one can form vesicles by reheating the tubules above T_m. As cooling cannot be avoided between the preparation stage and the observation, tubules can be considered as a mandatory intermediate step toward the formation of vesicles.

  Another, simpler method to prepare tubules has been proposed [14–16]. A few mg of $DC_{8,9}PC$ are dissolved in a few ml of ethanol. Adding doubly de-ionized water drop by drop leads to the formation of a white precipitate. The addition is stopped when complete precipitation of the tubules has taken place. The ethanol is then eliminated by: (i) centrifugation (10 000 tr.mn^{-1} during 15 mn), (ii) dissolution of the tubules and the remaining solvent in the same volume of doubly de-ionized water. Steps (i) and (ii) must be repeated until no traces of ethanol can be found. The tubules can then be heated as before to obtain vesicles.

  In the case of $DC_{8,9}PC$, a common remark concerning both methods has to be made: the vesicles, which are observed at a high temperature, go through an intermediate tubule stage. This means that vesicles made of $DC_{8,9}PC$ do not have to be separated from a lamellar phase: their membrane is formed by fusion and swelling of the small vesicles which appear when the tubule unwraps. For this reason, they are not subjected to the same kind of mechanical strains as in a standard swelling procedure. The result seems to

be a much higher fraction of vesicles of nontrivial topological genus. This is the reason why we mostly used this phospholipid in our study.

2.2. Observation and Analysis. — Observation is made at a constant temperature (± 0.05 °C) using a phase contrast microscope coupled to an image analysis system (512 × 512 pixel CCD camera, image acquisition card, personal computer). Vesicles are best seen when the tangent plane to their contour in the focal plane of the microscope is perpendicular to the focal plane: in this case the contrast of the contour with respect to the surrounding medium is maximized, and it appears as a dark line. Since vesicles are free to rotate under Brownian motion, pictures can be taken from different view points, thus leading to enough 2D contours to reconstruct the 3D surface of the vesicle.

It is, indeed, possible to digitize the experimental pictures and to build a triangulated geometrical model of the observed surface [17]. Using a computer program written by Brakke, the surface evolver [18], it is then possible to get the geometrical parameters (V, A and ΔA) of this triangulated surface, and to check by a direct minimization of the CEE whether it is or is not a stable or a metastable solution of one of the curvature models described previously.

Finally, in order to test the theoretical predictions concerning the various branches of solutions, we performed temperature-change experiments. This allows us to vary the reduced volume v of the vesicles, the volume being almost constant while the area changes as:

$$\frac{\mathrm{d}A}{\mathrm{d}T} = \gamma A, \tag{10}$$

where $\gamma \approx 4 \times 10^{-3}$ K^{-1}. A decrease of T thus corresponds to an increase of v.

3. Theoretical Predictions

Toroidal vesicles were first observed in the case of partially polymerized membranes [19, 20]. The observations we will report have been performed on *nonpolymerized*, i.e., fluid vesicles. In this case, the same theoretical analysis as for the spherical genus can be used, and predictions have been made within the framework of all preceding models (SC, BC and ADE).

Ou-Yang first noticed that the only circular toroidal solution of the SC model is characterized by a ratio of its generating circles, $\frac{R_2}{R_1} = \sqrt{2}$ (see Fig. 14), a torus known in the mathematical literature as the Clifford torus [21]. The stability analysis performed by Fourcade showed that it is a stable solution for any negative C_0, but that a positive C_0 makes it unstable to an axisymmetry-breaking deformation [22].

Seifert made the first systematic numerical calculations of axisymmetric toroidal shapes in the SC model for $C_0 = 0$ [23]. He predicted the possible existence of three distinct families of shapes, characterized by different kinds of cross sections: the almost circular tori (Ci) [24], the toroidal discocytes (called discoid tori in the following or Di), and the sickle-shaped tori (Si). The domain of existence of these shapes is limited to a finite interval on the reduced volume axis: for example, the circular tori are predicted to be unstable with respect to an axisymmetry-breaking deformation for $v > v_{\mathrm{Cliff}}$, where $v_{\mathrm{Cliff}} = 3/(2^{5/4}\sqrt{\pi}) \approx 0.71$ is the reduced volume of the Clifford torus.

In other words, one expects nonaxisymmetric shapes to occur for $v > v_{\mathrm{Cliff}}$. This prediction is related to the Willmore conjecture, first recalled by Duplantier [25]. The Willmore conjecture states that the Clifford torus is the absolute minimum of the CEE among surfaces of topological genus 1. But the CEE is invariant under 3D conformal transformations. These transformations (which preserve angles) contain not only rotations, translations and rescalings,

but also inversions. In contrast with the genus 0 case (all conformal transforms of the sphere are spheres), inversions are useful in the genus 1 case, because they generate a non-trivial one-parameter family of conformal transforms of the Clifford torus. These shapes known as Dupin cyclides are nonaxisymmetric and are also absolute minima of the CEE (see Appendix 8.4). As their reduced volume $v > v_{\text{Cliff}}$, they are the nonaxisymmetric shapes expected for $v > v_{\text{Cliff}}$ [23, 26].

In the case $C_0 \neq 0$, the existence of nonaxisymmetric shapes has been confirmed by Fourcade, who used a variational approach to study the stability of axisymmetric and non-axisymmetric shapes of the circular family for reduced volumes larger than v_{Cliff} [22].

A thorough analysis of the phase diagram for all three models has recently been done numerically by Jülicher, Seifert and Lipowsky (JSL) [27]. Systematically using special conformal transformations to test the stability of axisymmetric stable shapes, they have shown that nonaxisymmetric shapes should be observed for sufficiently high reduced volumes. The phase diagram of all models can be described using the three preceding families of characteristic shapes (Ci, Di and Si) plus a fourth one, the toroidal stomatocyte or stomatoid tori (St). Depending on the model and the region of the phase diagram, only one family (that of lowest energy) appears in the phase diagram, the other ones being metastable shapes [28]. The stomatoid tori do not appear as global minima (stable shapes) in the SC phase diagram. The ADE model (for $C_0 = 0$) slightly deforms the phase diagram of the BC model, depending on the value of the phenomenological parameter α, but remains qualitatively the same.

Four important results of this study (hereafter referred to as JSL) must be emphasized, with respect to the observations we will report:

- circular tori and sickle-shaped tori, both axisymmetric and nonaxisymmetric, are predicted in all three models (as stable or metastable shapes);
- stomatoid and nonaxisymmetric discoid tori are not predicted in the analysis of the SC model;
- nonaxisymmetric stomatoid tori are not predicted in the analysis of any model;
- finally, all the models predict a continuous transition from axisymmetric to nonaxisymmetric shapes by an increase of the reduced volume.

In the following, we present our observations for each family (almost circular, discoid, stomatoid and sickle-shaped) and discuss the compatibility of each model (described in detail in [27]) with our observations.

4. Circular Tori

4.1. Axisymmetric Circular Tori. — In the simplest model (SC with $C_0 = 0$), circular tori are expected to exist for any reduced volume smaller than $v_{\text{Cliff}} = 0.71$. Their cross section is expected to depart from a perfect circle by only a few percent, but we did not try to analyse this departure [22, 29].

We observed circular tori of reduced volume $0.3 < v < v_{\text{Cliff}}$ (see Fig. 1). Because of the Brownian rotation of the vesicles, we could take pictures of the vesicles at different orientations with respect to the optical axis of the microscope. We performed the geometrical mesurements (diameter of the hole, and diameter of the cross section) on the pictures when the symmetry axis of vesicle was either parallel or perpendicular to the optical axis [17]. Uncertainties in the reduced volume come mainly from the deviation from parallelism or perpendicularity of

Fig. 1. — Almost circular tori. Bar indicates 10 μm

the torus axis with respect to the optical axis of the microscope, but also from the thermal fluctuations, which slightly deform the shape (the relative uncertainty increases with the aspect ratio R_2/R_1 and never exceeded 5%). We estimated the reduced area difference Δa assuming that they were perfect circular tori, for which there exists an exact relation between v and Δa (see below).

4.1.1. Spontaneous Curvature Model. — Axisymmetric circular tori also exist for $C_0 \neq 0$ in the SC model. According to JSL, the maximum reduced volume $v^+(c_0)$ above which axisymmetry breaking is expected depends slightly on the reduced spontaneous curvature for $-1 < c_0 < 1$, and is close to v_{Cliff}. For this reason, we can say that the observed axisymmetric tori are compatible with a large range of spontaneous curvature and, as we do not know the spontaneous curvature of the phospholipids we use, we have no reason to assume a zero value.

According to JSL, for small reduced volume, sickle-shaped tori (Si) have a lower energy than circular tori (Ci). The frontier $v^-(c_0)$, below which Si tori are absolute minima of the energy, decreases with increasing c_0 ($v^-(0) = 0.58$, $v^-(2) = 0.3$). Our observations of circular tori with small reduced volume thus favor a large value for c_0 ($c_0 \geq 2$).

It is, however, worth recalling that *metastable* Ci tori exist for any reduced volume smaller than v^+. The frontier v^- between circular tori and sickle-shaped tori may thus not reflect an observable transition. Since the energy barrier between the two shapes (Ci and Si) exceeds $k_B T$ (it is of order $O(\kappa)$), this transition is unlikely to be driven by thermal fluctuations only.

4.1.2. Bilayer Coupling Model. — Almost circular tori are also predicted as global minima in this model. Using the parametrization of [21, 30] (see Fig. 14) for exactly circular tori, one gets:

$$v = \frac{3}{2\sqrt{\pi}} r^{-1/2}, \tag{11}$$

$$\Delta a = \frac{\sqrt{\pi}}{2} r^{1/2}, \tag{12}$$

$r = R_2/R_1$ being the ratio of the radii of the generating circles. As a result, exactly circular tori are represented by a curve $\Delta a_{\text{Ci}}(v)$ in the $(v, \Delta a)$ plane whose equation is:

$$\Delta a_{\text{Ci}}(v) = \frac{3}{4v}. \tag{13}$$

In the phase diagram of the BC model calculated by JSL, shapes of a given Δa are predicted to be nonaxisymmetric if $v > v_{\text{Ci}}$, and to look more like discoid tori when $v < v_{\text{Ci}}$.

The abundance of the observed circular tori as compared to the other classes (see below the corresponding Sects.) would thus imply that, for an unknown reason, a particular, narrow region of the phase diagram (around the line $\Delta a_{C_1}(v)$) is favored. Unless we find a plausible physical reason for this selection, we may conclude that the BC model looks more restrictive than the SC model, as far as our observations of circular tori are concerned.

Let us consider a possible explanation of this selection: the BC model assumes a strict conservation of the monolayer area difference, which is a reasonable hypothesis only on short time scales (shorter than the typical flip-flop time constant [31]). If one observes the vesicles a sufficiently long time after their formation (which is the case when vesicles are observed after a week), exchange of lipids between the two monolayers is likely to have occurred in order to reach a value of Δa which minimizes E_0, Equation (1) (at fixed reduced volume, the exchange rate with the bulk solution being negligible). We are thus led to consider two different physical problems:

- *A short-time-scale problem*: given the geometrical characteristics of a vesicle, v and Δa, determine the stable equilibrium shape of the vesicle. The answer to this problem is given by the phase diagram as calculated by JSL in [27]. One must also consider the formation process, which might favor specific solutions.

- *A long-time-scale problem*: given the geometrical constraint v (plus the total area of both monolayers), determine the stable equilibrium shape of the vesicle, allowing for a redistribution of phospholipids between the two monolayers. In this case, consideration of the starting shape is essential, a vesicle evolving towards the nearest accessible local minimum.

Let us try to perform the second analysis using a curve calculated by JSL in reference [27]. They give a detailed description of the metastable equilibrium axisymmetric shapes and their energy as a function of Δa for the particular value $v = 0.55$ (Fig. 1 of [27], simplified in Fig. 2).

For $v = 0.55$, three distinct shapes have a locally minimal elastic energy E_0: a sickle-shaped torus ($\Delta a_{S_1} \approx 0.5$), a discoid torus ($\Delta a_{D_1} \approx 1.1$) and a circular torus ($\Delta a_{C_1} \approx 1.4$). The elastic energy barriers separating these three minima are of the order of $0.6 - 1.2\kappa$ (where $\kappa \approx 10 - 20 k_B T$), so that we expect these minima to be well separated attractors for the shapes with neighbouring Δa and identical v. Δa will evolve (increase or decrease) to the nearest local minimum, hence all tori with $v = 0.55$ and $\Delta a(t = 0) > 1.25$ will evolve to the circular torus. This picture probably qualitatively holds for all $v < v_{\text{Cliff}}$.

In summary, our observations of a majority of circular axisymmetric tori are compatible with the predictions of the BC model, taking into account the possible redistribution of phospholipids between the two monolayers on a long time scale.

4.1.3. Area Difference Elasticity Model. — In principle, as the ADE model interpolates between the two preceding models, we might hope that it has their advantages without having their drawbacks. In fact, because it depends on a phenomenological parameter α that we cannot measure (see for example [9]), and is expected to vary from vesicle to vesicle depending on their composition or lamellarity [11], there are as many phase diagrams as there are vesicles. In the following, we discuss the case treated in [27], $\alpha = 1$, $C_0 = 0$. The geometrical parameters are v and Δa_0, the equilibrium reduced area difference.

As stated before, we did not try to measure Δa (which should be close to Δa_0). In fact, as this model predicts that circular tori are stable for a rather broad range of Δa_0 (at least for $\alpha = 1$), for a given reduced volume, this model is less restrictive than the BC model considered previously, as far as axisymmetric circular tori are concerned.

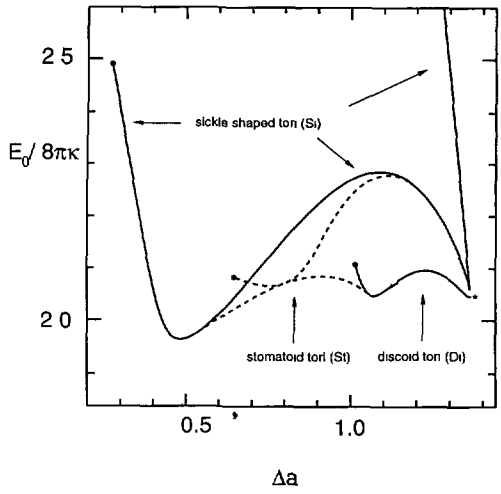

Fig. 2. — Curvature elastic energy E_0 of equilibrium shapes of reduced volume $v = 0.55$. Three families are present· the sickle shaped tori (Si), the stomatoid tori (St, dashed curves) and the discoid tori (Di). The curves end at points where the inner radius of the hole shrinks to zero. There are three local minima That indicated by a star corresponds to an almost circular tori, which is the limiting axisymmetric shape: shapes with greater Δa are nonaxisymmetric, but have higher energy. Adapted from reference [27].

An interesting fact about the ADE model is that axisymmetric circular tori of reduced volume slightly larger than v_{Cliff} (up to $v^+ = 0.77$ for $\alpha = 1$) are expected. Taking this prediction into account, we cannot explain why we observed no axisymmetric circular tori of reduced volume $v > v_{\text{Cliff}}$, unless the phenomenological parameter α is large, which makes it only slightly different from the BC model.

4.2. The Clifford Torus. — In the case of the Clifford torus ($v_{\text{Cliff}} = 0.71, \Delta a_{\text{Cliff}} = 2^{-3/4}\pi^{1/2} \approx 1.05$), we sometimes observed marked thermal fluctuations. Figure 3 shows different views some seconds apart of the same torus: the axisymmetry is slightly broken by fluctuations, as well as the circular shape of the hole, the mean shape being a Clifford torus [32]. These marked fluctuations, which do not exist for most of the Clifford tori we observed, may be related to the near degeneracy of the ground state of the SC model for $C_0 = 0$ and $v = v_{\text{Cliff}}$, as described by Fourcade [22].

Let us recall these results: following a conjecture due to Willmore, the Clifford torus is the genus 1 shape which absolutely minimizes the CEE. By conformal invariance of the CEE, shapes obtained by an inversion of the Clifford torus have also the same energy, and thus minimize the CEE. This conformal degeneracy is, however, broken by the reduced volume constraint. Nevertheless, it is possible to couple two other kinds of deformations to this conformal mode, in order to satisfy the reduced volume constraint to leading order. This leads to the remarkable result that the energy of such a deformed Clifford torus is constant up to fourth order in the relative amplitude of the deformation a^*.

This result does not hold for $C_0 \neq 0$. For a positive spontaneous curvature, the corresponding *equilibrium shape is non-axisymmetric* [22, 23]. For $-1 < c_0 < 0$, the Clifford torus is the equilibrium shape, but the conformal mode has now an energy quadratic in a^*, like any other deformation mode.

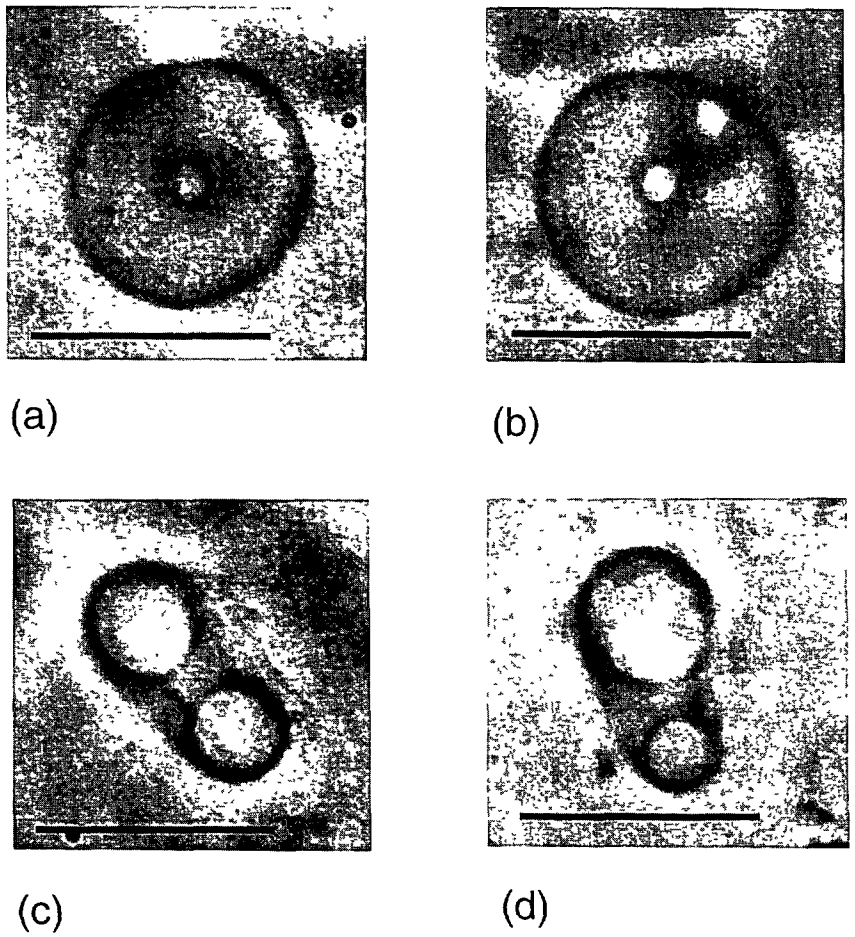

Fig 3. — Fluctuating Clifford torus. Bar indicates 10 μm.

In Figure 3, we can estimate a^* *via* the eccentricity of the hole (see Appendix 8.4). From our observations, we mesure a relatively large amplitude $a^* = \frac{a}{R_1} \approx 0.22$, where R_1 is the inner radius of the unperturbated Clifford torus. For $\kappa \approx 20 k_B T$, the energy of this deformation (if $C_0 = 0$) is:

$$\Delta E_0 = 8\pi^2 \kappa (a^*)^4 \approx 3 \pm 1 k_B T, \tag{14}$$

which is compatible with a thermal excitation of this mode.

Its energy in the case of a negative reduced spontaneous curvature $c_0 < 0$ would be:

$$\Delta E_{SC} = -2^{9/4} \pi^{3/2} c_0 \kappa (a^*)^2 \approx -25 c_0 k_B T. \tag{15}$$

One has thus to assume a small value of the reduced spontaneous curvature ($|c_0| \ll 1$) in order to explain the thermally excited fluctuations observed.

The particular value, $C_0 = 0$, necessary for such a conformal near degeneracy could explain the rare occurrence of this phenomenon.

In the BC model, there exists another constraint, ΔA, which plays the role of a spontaneous curvature. Extending the analysis of Fourcade, it can be shown that one cannot satisfy this

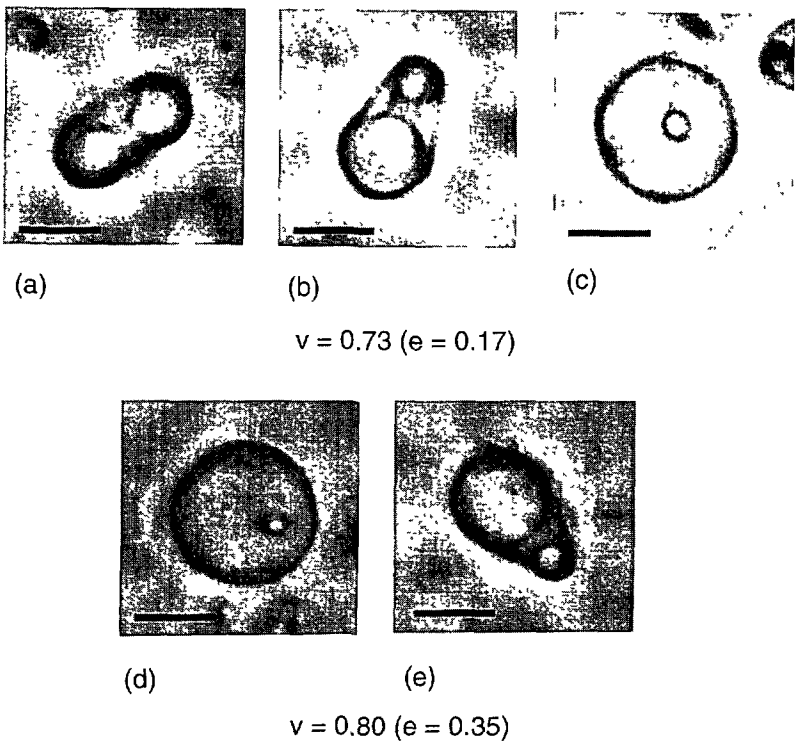

Fig. 4. — Nonaxisymmetric circular tori or Dupin cyclides. (a) Front view (b) side view (c) top view (d) top view (e) side view. Bar indicates 10 μm.

second constraint by coupling to another deformation mode [33]. The observation of one case of marked conformal fluctuations of the Clifford torus might, thus, be an argument against the BC model.

4.3. Nonaxisymmetric Circular Tori. — Nonaxisymmetric circular tori are the only genus 1 vesicles we observed having a reduced volume $v > v_{\text{Cliff}}$ up to $v = 0.92$ (see Fig. 4). To determine their reduced volume, we used the same procedure (described above) as for the axisymmetric tori: geometrical characteristics (diameter of the hole, external diameter of the vesicle, distance of the hole center from the external contour center) were measured when the symmetry plane of the vesicle was either parallel or perpendicular to the focal plane. We assumed that their shapes were close to those of Dupin cyclides (see Fig. 14), which yields the reduced volume *via* formula (A.4). This approximation is justified by the circularity of the cross sections of the tori, a characteristic of Dupin cyclides. Uncertainty on the reduced volume is likewise smaller than 5%.

A more easily calculated geometrical parameter, in the case of non-Dupin cyclides, is the eccentricity given by formula (A.2), which tells how excentric the hole is.

These observations of Dupin cyclides with reduced volumes ranging 0.71 to 0.92 can be discussed within the framework of each model.

4.3.1. Spontaneous Curvature Model. — For $c_0 > -1$, all vesicles of a reduced volume larger than $v^+(c_0)$ are expected to be nonaxisymmetric. According to JSL, $v^+(0) = v_{\text{Cliff}}$, $v^+(1) =$

0.68 and $v^+(2) = 0.63$. As we have not seen quasi Dupin cyclides of reduced volume smaller than v_{Cliff}, we infer that the reduced spontaneous curvature was small.

4.3.2. Bilayer Coupling Model. — In the framework of the BC model, each vesicle is characterized by a second geometrical parameter, its reduced area difference Δa. According to JSL, for $\Delta a > \Delta a_{\text{Cliff}} = 1.054$, the line of axisymmetric circular tori builds up the frontier between axisymmetric and nonaxisymmetric tori. Dupin cyclides continue this line inside the nonaxisymmetric region, for smaller reduced area difference. As we have not been able to quantify the difference of the observed vesicles with exact Dupin cyclides, our observations would likewise imply that, for some reasons, only vesicles around this particular line have been observed. Using the calculations of JSL, a possible explanation of this fact might involve a redistribution of phospholipids between both monolayers (flip-flop) on a sufficiently long time scale, as argued in Section 4.1.2.

The analysis of Section 4.2.2 can be reproduced using the results of JSL: for $v = 0.73 > v_{\text{Cliff}}$, the shape with the smallest CEE is the Dupin cyclide of reduced volume v (there is a single minimum in contrast to the cases $v < v_{\text{Cliff}}$). On a sufficiently long time scale, one can, thus, expect a redistribution of the molecules between the two monolayers which drives any shape of reduced volume $v > v_{\text{Cliff}}$ toward this minimum. This would explain the exclusive observation of quasi-Dupin cyclides for reduced volume $v > v_{\text{Cliff}}$.

4.3.3. Area Difference Elasticity Model. — The phase diagram published in reference [27] corresponds to the particular values $\alpha = 1$, $C_0 = 0$. For these values, the line of Dupin cyclides occurring in the phase diagram of the BC model might be enlarged (similarly to the Clifford torus, which appears to be the stable equilibrium shape for $0.8 < \Delta a_0 < 1.054$). In this case, our observation of Dupin cyclides would be less surprising. two apparently identical vesicles could correspond to two different Δa_0 (the actual reduced area difference Δa being identical).

In summary, our observations of Dupin cyclides are compatible with the three models. In the case of the BC model, one has, however, to look for specific reasons (flip-flop on long time scale or selection *via* the formation process) to explain the selection of a single line in the phase diagram.

4.4. Temperature Variations and Axisymmetry Breaking. — The preceding observations were done at constant temperature. In order to get more information on the validity of all the models, we performed temperature variation experiments.

As recalled by Berndl *et al.* [13], one of the effects of a temperature variation is a modification of the reduced volume:

$$v(T) = v(T_0)\, \mathrm{e}^{-\frac{3}{2}\gamma(T-T_0)}, \tag{16}$$

where T_0 is the initial temperature and γ the thermal area expansivity of the bilayer (of the order of 4×10^{-3} K^{-1} for most phospholipids).

In the framework of the BC model, the other effect of a temperature variation is a modification of the reduced area. If one assumes that the volume of the bilayer remains constant, the reduced area difference behaves in the opposite way, so that:

$$v(T)\, \Delta a(T) = v(T_0)\, \Delta a(T_0). \tag{17}$$

Another simple hypothesis is that the distance between the two monolayers remains constant. In this case, (17) changes into:

$$v(T)\, \Delta a(T)^3 = v(T_0)\, \Delta a(T_0)^3. \tag{18}$$

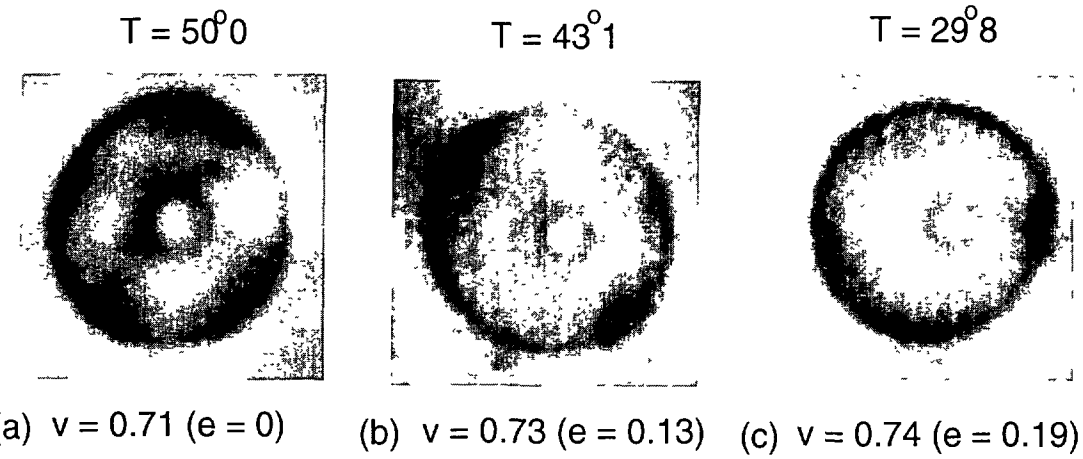

Fig. 5. — Observed equilibrium shapes during a temperature-variation experiment. The temperature is stabilized during each observation.

Finally, it has been proposed that the two monolayers may have slightly different thermal expansivities. Assuming that the volume of the bilayer remains constant, one has:

$$v(T)\Delta a(T) = v(T_0)\left(\Delta a(T_0) + b\left(\left[\frac{v(T_0)}{v(T)}\right]^{\frac{2}{3}\epsilon} - 1\right)\right), \tag{19}$$

where b is of the order of 10^3 for common vesicles, and ϵ is the relative asymmetry of the thermal expansivities:

$$\gamma_{\text{in}} = \gamma_{\text{out}}(1+\epsilon). \tag{20}$$

In the framework of the SC model, the dependence of C_0 on the temperature is not known. The simplest hypothesis is that it is temperature independent.

The main interest of temperature variation experiments is to test the connection between the axisymmetric branch of the circular tori and its nonaxisymmetric branch. As the Clifford torus stays on the frontier between axisymmetric and nonaxisymmetric shapes in all phase diagrams, we focused our attention on this particular shape. Figure 5 shows the corresponding typical experiment.

Our observations show that a decrease of the temperature induces an increase of the reduced volume, as measured *via* the parameters of the Dupin cyclides. The shape transformations are reversible. Formula (16) leads to a thermal expansivity $\gamma = (1.5 \pm 0.5) \times 10^{-3}$ K^{-1} for $DC_{8,9}PC$.

These observations call for some comments with respect to the theoretical models.

4.4.1. Spontaneous Curvature Model. — In the SC model and for a small reduced spontaneous curvature, the Clifford torus is expected to lie on or near the frontier between axisymmetric and nonaxisymmetric shapes, depending on its spontaneous curvature: an increase of its reduced volume leads anyway to an axisymmetry breaking, as is, indeed, observed. Measurement of the spontaneous curvature should be in principle possible in this kind of experiment: once in the nonaxisymmetric region, a decrease of the reduced volume leads back to the axisymmetric region through a limiting shape whose reduced volume is related to the spontaneous curvature.

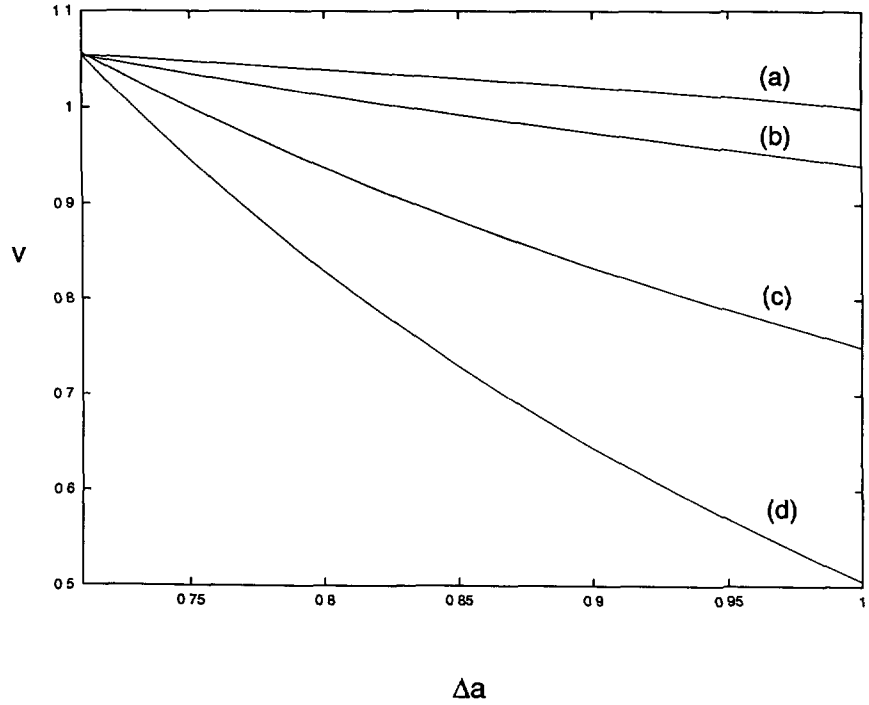

Fig. 6 — Temperature trajectories of a Clifford torus in the BC model. (a) corresponds to the cyclide family, (b) to the constant inter-monolayer distance hypothesis (Eq (18)), (c) to the constant bilayer volume hypothesis (Eq. (17)) and (d) to Equation (19) with $b = 1000$, $\epsilon = 1.5 \times 10^{-3}$.

In all the experiments we performed on different vesicles, the last axisymmetric shape was a Clifford torus (with an uncertainty on the measured reduced volume smaller than 5%, as discussed before, which implies $|c_0| < 1$).

4.4.2. Bilayer Coupling Model. — In the BC model, a decrease of the reduced volume of the Clifford torus let it follow a trajectory in the $(v, \Delta a)$ plane which depends on the corresponding Δa variation. Figure 6 shows the Dupin cyclide curve and three trajectories corresponding to Equations (17, 18 and 19) with $\epsilon = 1.5 \times 10^{-3}$. However, due to the small thermal expansivity of the phospholipids, the maximum reduced volume attained in the experiment of Figure 5 is $v = 0.74$. For this value, the three distinct shapes corresponding to the three theoretical trajectories and the Dupin cyclide are experimentally indistinguishable. For this reason, our observations are not in contradiction with the BC model.

4.4.3. Area Difference Elasticity Model. — As discussed before, the ADE model in principle permits the constraints of the first two models to be softened. It should also allow observations in which a temperature decrease does not necessarily lead to the axisymmetry breaking of the Clifford torus (at least over a reasonable range of temperatures). Up to now, we have not observed such a phenomenon.

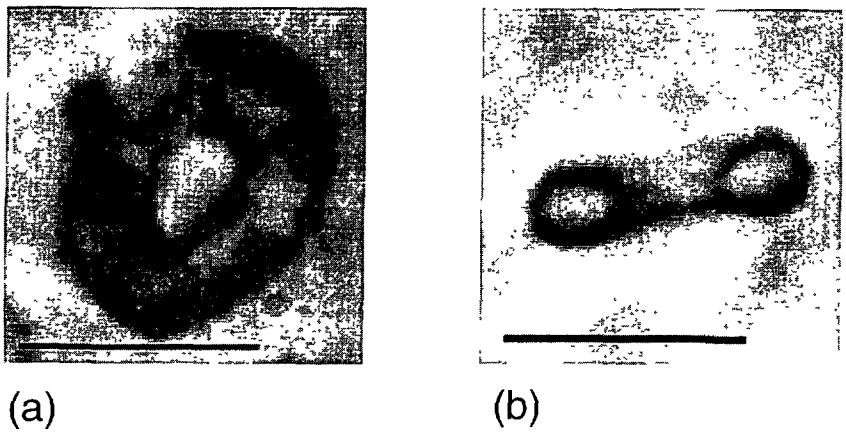

Fig. 7. — Axisymmetric discoid torus. Bar indicates 10 μm.

5. Discoid Tori

Discoid tori occupy a broad region in the phase diagrams of both BC and ADE models. They exist as metastable states in the SC model.

5.1. AXISYMMETRIC DISCOID TORI. — We observed some axisymmetric discoid tori, an example of which is shown in Figure 7. Using the procedure described in Section 2, we get the following parameters of the vesicle: $(v, \Delta a) = (0.51, 1.37)$. The stability of this shape can be tested numerically, using the surface evolver program. With a constraint on v, and no constraint on Δa, one ends up with an almost circular torus with $\Delta a = 1.46$ and energy $\frac{E_0}{8\pi\kappa} = 2.31$ (see Fig. 8a), in agreement with previous calculations of Seifert [23].

With a constraint on Δa, one ends up with the shape shown in Figure 8b. Its energy $\frac{E_0}{8\pi\kappa} = 2.35$ is slightly higher than the calculations of Seifert for the discoid family [23, 34].

The result of the equilibration process gives the Lagrange parameters corresponding to the three constraints $(A, V, \Delta A)$. This permits us to get the equivalent reduced spontaneous curvature, $c_0 = -0.04$, within the BC model. The shape of Figure 8 is thus also a solution of the SC model for $(v, c_0) = (0.51, -0.04)$. However, as shown by JSL, for these values, the stable shape belongs to the sickle-shaped family: the observed vesicle is a metastable state of the SC model.

5.2. NONAXISYMMETRIC DISCOID TORI. — We also observed a few nonaxisymmetric tori, although this kind of shape did not appear in the predictions of JSL. An example of such a vesicle is shown in Figure 9.

The same procedure as before yields $(v, \Delta a) = (0.52, 1.19)$. In this case, equilibration of the surface with a single constraint on v leads to a nonaxisymmetric shape, shown in Figure 10a. It is very close to, but different from, the observed vesicle ($\Delta a = 1.07$, $\frac{E_0}{8\pi\kappa} = 2.16$). Taking into account the constraint on Δa, one gets the non-axisymmetric shape shown in Figure 10b ($\frac{E_0}{8\pi\kappa} = 2.21$), which is very similar to the observed vesicle.

5.3. DISCUSSION. — Within the BC model, the expected shape for this set of parameters is an axisymmetric discoid torus. But, the existence of a nonaxisymmetric discoid torus is not

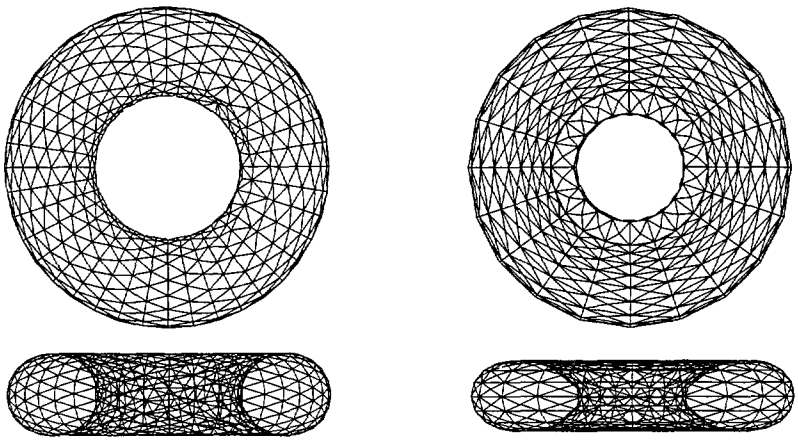

Fig. 8. — Numerical model of the vesicle of Figure 7 after equilibration. (a) With constraint on v only: $v = 0\,51$, $\Delta a = 1\,41$, $\frac{E_0}{8\pi\kappa} = 2.31$.(b) With constraint on v and Δa: $v = 0.51$, $\Delta a = 1.37$, $\frac{E_0}{8\pi\kappa} = 2.35$.

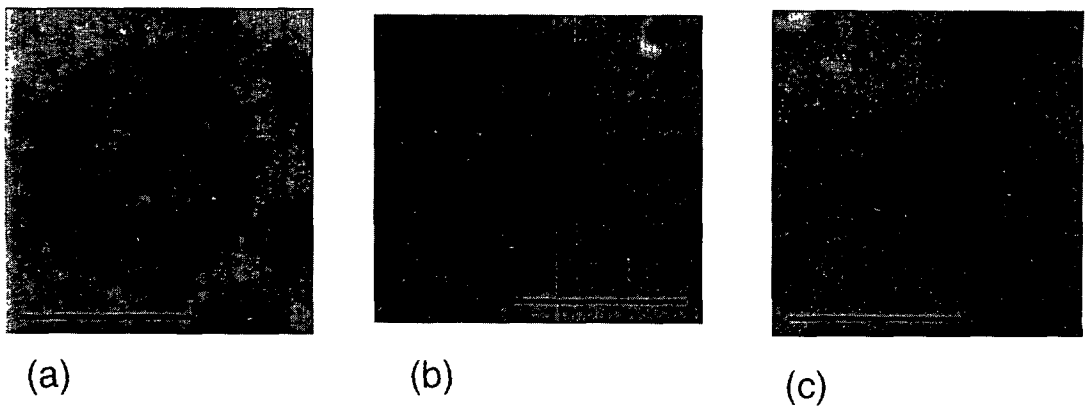

Fig. 9. — Nonaxisymmetric discoid torus. (a) top view (b) side view (c) front view. Bar indicates 10 μm.

surprising, if one considers the calculations made by Seifert [23]. He showed that there exists a branch of axisymmetric discoid tori which is unstable with respect to axisymmetry breaking for $v < 0.58$: the observed vesicle could thus be the resulting stable nonaxisymmetric shape. Its energy is perfectly compatible with this hypothesis.

As in the previous example, the same result can be obtained within the SC model with the appropriate spontaneous curvature, instead of the Δa constraint. One gets $c_0 = -0.82$. According to JSL, one expects a nonaxisymmetric equilibrium shape for these values, although they predict that it should belong to the sickle-shaped family. The observed vesicle might thus be a metastable shape of the SC model.

Within the ADE model ($\alpha = 1$ and $c_0 = 0$), almost all shapes with $v = 0.52$ are expected to be axisymmetric. For Δa_0 close to $\Delta a = 1.19$, the stable shape belongs to the discoid family.

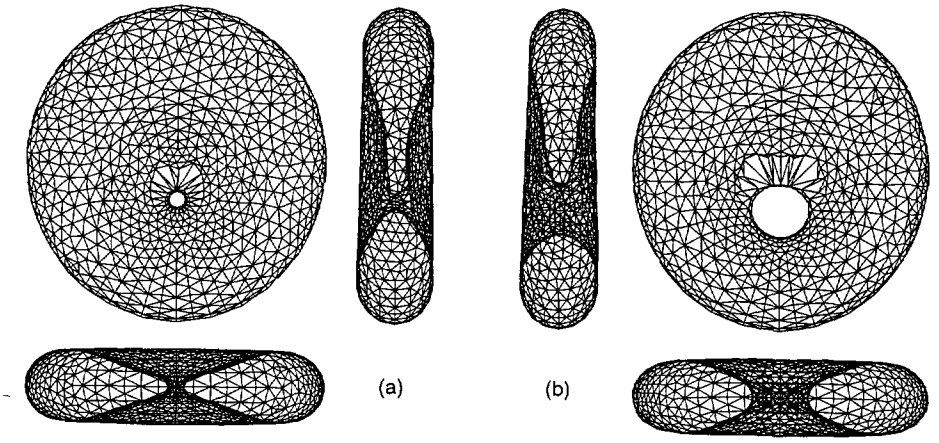

Fig. 10. — Two numerical models of the vesicle of Figure 9, equilibrated (a) with a reduced volume constraint only: $v = 0.52$, $\Delta a = 1.07$, $\frac{E_0}{8\pi\kappa} = 2.16$ (b) With both reduced volume and reduced area difference constraints: $v = 0.52$, $\Delta a = 1.19$, $\frac{E_0}{8\pi\kappa} = 2.21$.

For $\Delta a_0 > \Delta a$, it belongs to the circular family; and for $\Delta a_0 < \Delta a$, to the stomatoid family. The observed vesicle might thus be a metastable shape of this ADE model (we did not make any calculations).

These observations show that the discoid tori can be produced by the formation processes we used, although at a lower rate compared to the circular tori. The existence of nonaxisymmetric discoid tori, which are not predicted by JSL [35], also shows that their axisymmetry-breaking stability test might not be sufficient to explore the nonaxisymmetric region of the phase diagrams. Indeed, the shapes of Figure 10 cannot be made axisymmetric by conformal transformations.

This could also suggest that the use of infinitesimal conformation modes to determine the stability of axisymmetric shapes with respect to axisymmetry-breaking modes is not sufficient. As a consequence, the phase boundaries between axisymmetric and nonaxisymmetric regions could be shifted towards smaller reduced volume.

6. Stomatoid Tori

Figure 11 shows a nonaxisymmetric stomatoid torus.

We digitized this shape, as previously explained, in order to build a triangulated approximation. The surface evolver program yields the following parameters: $(v, \Delta a) = (0.70, 1.05)$. With a single constraint on v, the surface relaxes to an almost circular torus of the same reduced volume. With a second constraint on Δa, the surface remains stable, see Figure 12.

6.1. Discussion. — For this set of parameters, JSL predict within the BC model an axisymmetric torus lying on the frontier between discoid and stomatoid tori, and not far from the region of nonaxisymmetric shapes. Our observation is thus partially in agreement with this prediction (the vesicle seems to be close to both families and is only slightly nonaxisymmetric).

Once again, it is possible to get the same metastable shape within the SC model by minimization of (3) with a constraint on v and a reduced spontaneous curvature $c_0 = 1.55$, obtained

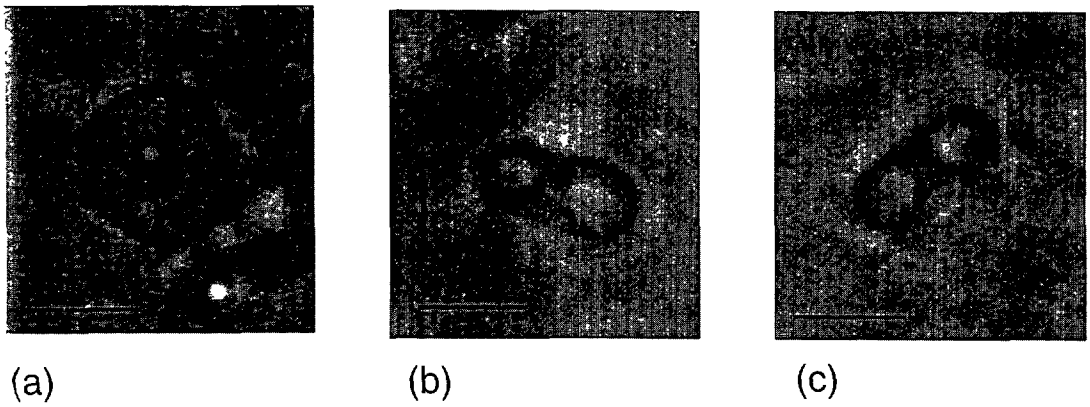

Fig. 11. — Nonaxisymmetric stomatoid vesicle. (a) Top view (b) side view (c) front view Bar indicates 10 μm.

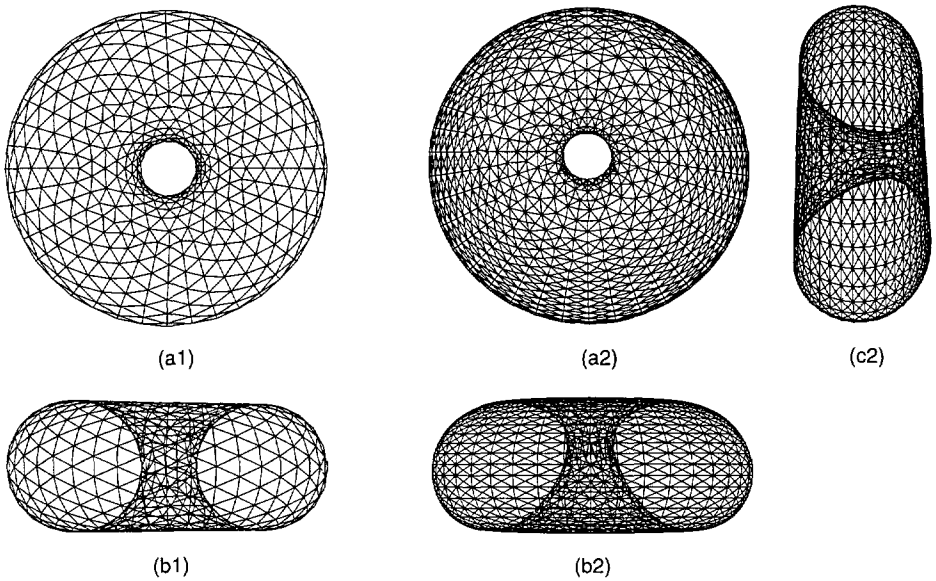

Fig. 12. — Numerical models of the vesicle of Figure 11 equilibrated with the surface evolver program Left, under reduced volume constraint only. $v = 0.70$, $\Delta a = 1.06$, $\frac{E_0}{8\pi\kappa} = 1.59$. Right, under both reduced volume and reduced area difference constraints. $\Delta a = 1\ 05$, $\frac{E_0}{8\pi\kappa} = 1.60$. (a) Top view, (b) front view, (c) side view.

via the Lagrange parameters of the preceding calculation. For this set of parameters, the stable shape within the SC model is expected to be nonaxisymmetric and not far from the circular family.

Within the ADE model discussed in JSL, stable shapes with $v = 0.70$ and Δa_0 close to $\Delta a = 1.05$ should be very close to the Clifford torus, which is not the case. For $\Delta a_0 > \Delta a$, one expects nonaxisymmetric shapes but with no up/down symmetry breaking (i.e., non-stomatoid). For $\Delta a_0 < \Delta a$, there is only a very narrow region of stable stomatoid tori, which

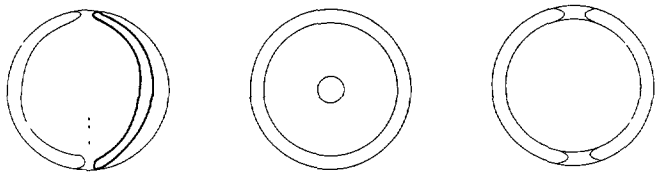

Fig. 13. — Schematic representation of a sickle-shaped torus (a) Perspective of a partially open shape (b) top view (c) side view.

are, moreover, axisymmetric. The observed vesicle might thus be a metastable shape of this model.

These observations show that the stomatoid tori can be produced by the formation processes we used, although, again, at a lower rate compared to the circular tori. The observation of a nonaxisymmetric stomatoid torus, which is not predicted by JSL, confirms that the axisymmetry-breaking stability test is not sufficient to explore the nonaxisymmetric region of the phase diagrams.

7. Comment on the Predicted Sickle-Shaped Tori

Sickle-shaped tori (axisymmetric or non-axisymmetric) are predicted to be stable shapes in all three models. In fact, we observed no such vesicle. However, we reported elsewhere the observation of genus 2 vesicles (topologically equivalent to 2-hole tori) of the sickle-shaped kind [36]: they look like two concentric spheres connected by three tube-like passages. This is similar to the expected appearance of the sickle-shaped tori (two spheres connected by two tube-like passages). Thermal fluctuations of these passages, as described in reference [36], are, however, expected to destroy the axisymmetry of genus 1 sickle-shaped vesicles.

These thermal fluctuations have a crucial experimental consequence. Sickle-shaped tori have two characteristic aspects when observed with a phase contrast microscope (see Fig. 13). The first one corresponds to an observation parallel to the symmetry axis of the vesicle: one should see two concentric nearby circles plus a smaller one in the center (the inner contour of the two holes viewed one above the other). The second one corresponds to an observation perpendicular to the symmetry axis: one should see again two concentric nearby circles, connected by two tube-like passages. However, the probability of these two configurations is very low, due to the Brownian rotation of the vesicles and to the thermal fluctuations of the passages.

For these reasons, we believe that sickle-shaped tori probably exist, but they will be fairly difficult to observe.

8. Summary

The preceding observations have shown the existence of three (circular, discoid and stomatoid tori) of the four expected families of toroidal vesicles. The fourth one (sickle-shaped tori) has not been observed, but related observations of vesicles of higher genus lead to the conclusion that it probably exists, but might be difficult to observe for experimental reasons.

A systematic analysis of the observed vesicles in terms of triangulated surfaces allows one to determine their geometrical parameters and to test the stability of these shapes within the

SC and BC models. These values were used to compare our observations with the theoretical predictions.

The main results of this study are the following.

8.1. CIRCULAR TORI. — Within the BC model, the relatively high frequency of circular tori calls for a explanation in terms of *phospholipid redistribution between the two monolayers of the membrane on long time scales.*

Within the SC model, the same observation favors either a broad range of spontaneous curvature or the *observability of metastable shapes.*

8.2. NONAXISYMMETRIC DISCOID AND STOMATOID TORI. — Observations of nonaxisymmetric discoid and stomatoid tori, which were not predicted, show that *the symmetry-breaking modes of discoid tori and of stomatoid tori cannot be approximated by infinitesimal conformal transformations.* Since the phase boundaries of axisymmetry breaking in the work of JSL are lower bounds on the regions of stable nonaxisymmetric shapes, this region of the phase diagram may be shifted toward smaller reduced volumes (see Ref. [27]).

8.3. AXISYMMETRY BREAKING. — The temperature-variation experiments performed on the Clifford torus, which lead to the axisymmetry breaking, show that *the curvature elastic energy is, indeed, conformally invariant.* This property might also explain strong fluctuations of some Clifford tori observed at constant temperature.

8.4. COMPARISONS BETWEEN MODELS. — We cannot exclude any of the three models. The SC model is compatible with our observations, provided one takes into account that metastable shapes can be observed. The BC model predicts a much richer zoology than the observed one, a fact which might be due to the redistribution of phospholipids between monolayers on a long-time scale. Finally, the ADE model, which smoothly interpolates between them is, of course, compatible with our observations.

Acknowledgments

We greatly benefited from discussions with Frank Jülicher, Udo Seifert and Reinhard Lipowsky, whom we thank for the kind permission to use Figure 2 adapted from reference [27]. We thank Bertrand Fourcade for fruitful discussions. We are grateful to Vincent Croquette for his kind help in the image processing part of this work. Kenneth Brakke kindly discussed the subtleties of his surface evolver program.

Appendix A

Geometrical Results

A.1. PARAMETRIZATION OF THE AXISYMMETRIC TORI AND DUPIN CYCLIDES. — The parametrization of the Dupin cyclides can be obtained by different means (see for example) [37, 38]. Here we follow Ou-Yang [30]:

$$\begin{cases} x &= \left(r(c - a\cos\theta\cos\psi) + b^2\cos\theta\right)/D, \\ y &= b\sin\theta(a - r\cos\psi)/D, \\ z &= b\sin\psi(c\cos\theta - r)/D, \\ D &= a - \cos\theta\cos\psi \end{cases} \tag{A.1}$$

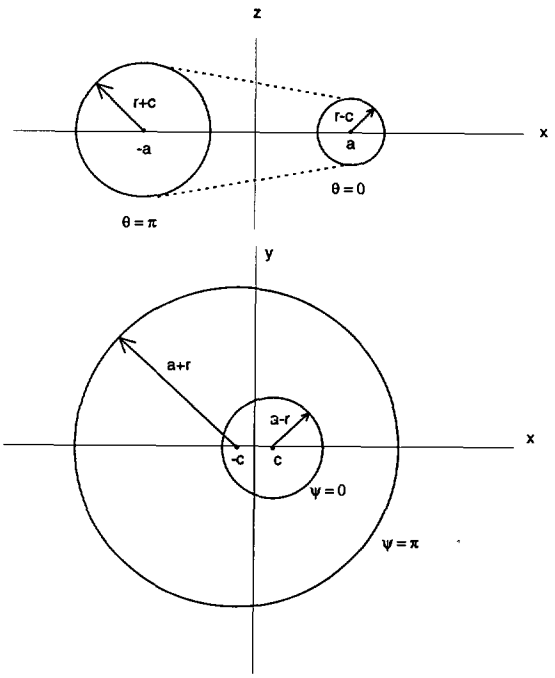

Fig. 14. — Parametrization of the Dupin cyclides.

where $\theta \in [0, 2\pi]$, $\psi \in [0, 2\pi]$ and $c = \sqrt{a^2 - b^2}$.

The meaning of the other parameters can be read from Figure 14.

The eccentricity is defined by:

$$e = \frac{c}{a} \tag{A.2}$$

and can easily be deduced from the top and side views of the cyclide (see Fig. 14).

The observable Dupin cyclides are conformal transforms of the Clifford torus, which lead to the relation:

$$r = \sqrt{\frac{a^2 + c^2}{2}}. \tag{A.3}$$

Starting from formula (A.1), one gets the reduced volume of the observable Dupin cyclides (see Fig. 15):

$$v(e) = \frac{3}{2\sqrt{\pi}}(1 - e^2)^{-1/2} \left[\frac{1 + e^2}{2} G_1(e) + \frac{e^2}{2} G_2(e)\right] \left(\sqrt{\frac{1 + e^2}{2}} G_1(e)\right)^{-3/2}, \tag{A.4}$$

where:

$$G_1(x) = F\left(\frac{3}{2}, \frac{1}{2}, 1; x^2\right) + \frac{1}{2} x^2 F\left(\frac{3}{2}, \frac{3}{2}, 2; x^2\right), \tag{A.5}$$

$$G_2(x) = F\left(\frac{1}{2}, \frac{3}{2}, 2; x^2\right) + \frac{1}{2} x^2 F\left(\frac{3}{2}, \frac{5}{2}, 3; x^2\right). \tag{A.6}$$

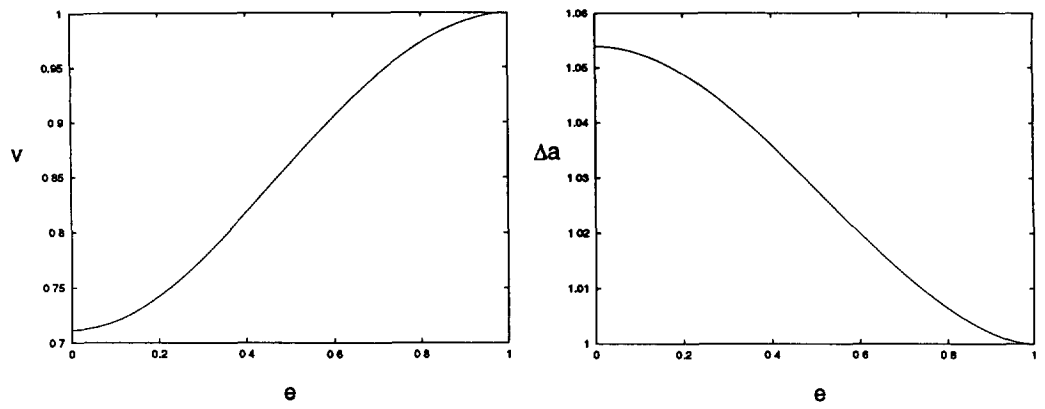

Fig. 15. — Reduced volume and reduced area difference of the Dupin cyclides as a function of their eccentricity.

Similarly, the reduced area difference reads:

$$\Delta a(e) = \sqrt{\frac{\pi}{2}} \left(\frac{1-e^2}{1+e^2} \right)^{1/2} \left(2F\left(\frac{1}{2}, \frac{3}{2}, 1; e^2 \right) - F\left(\frac{1}{2}, \frac{1}{2}, 1; e^2 \right) \right). \tag{A.7}$$

The axisymmetric tori are a subset of this family, characterized by a zero eccentricity ($e = 0$). One defines the two radii of the generating circles by $R_1 = r$ and $R_2 = a$.

A.2. Special Conformal Transformations. — Special conformal transformations build a subgroup of the conformal transformations, defined by $\imath \circ t_{\mathbf{a}} \circ \imath$, where $\imath$ is the unit sphere inversion:

$$\mathbf{r}' = \frac{\mathbf{r}}{\mathbf{r}.\mathbf{r}} \tag{A.8}$$

and $t_{\mathbf{a}}$ the translation of vector $\mathbf{a}$.

A.3. Fluctuations of the Clifford Torus. — To study the fluctuations of the Clifford torus, we use the toroidal coordinates introduced by Fourcade [22]. An axisymmetric torus is defined by a real parameter η:

$$\begin{cases} x = \dfrac{\sinh\eta\cos\phi}{\cosh\eta - \cos\theta}, \\ y = \dfrac{\sinh\eta\sin\phi}{\cosh\eta - \cos\theta}, \\ z = \dfrac{\sin\theta}{\cosh\eta - \cos\theta}, \end{cases} \tag{A.9}$$

where $\cosh\eta = \sqrt{2}$ for the Clifford torus (see Fig. 16 for the definition of θ and ϕ).

As shown in reference [22], the almost conformal mode has the following effect on each point M$\rightarrow$ M$'$ of the Clifford torus:

$$\overrightarrow{\mathrm{MM}'} = \frac{\delta\eta(\theta,\phi)}{\cosh\eta - \cos\theta}\mathbf{n}, \tag{A.10}$$

where $\mathbf{n}$ is the exterior normal of the Clifford torus, and

$$\delta\eta(\theta,\phi) = a\cos\phi. \tag{A.11}$$

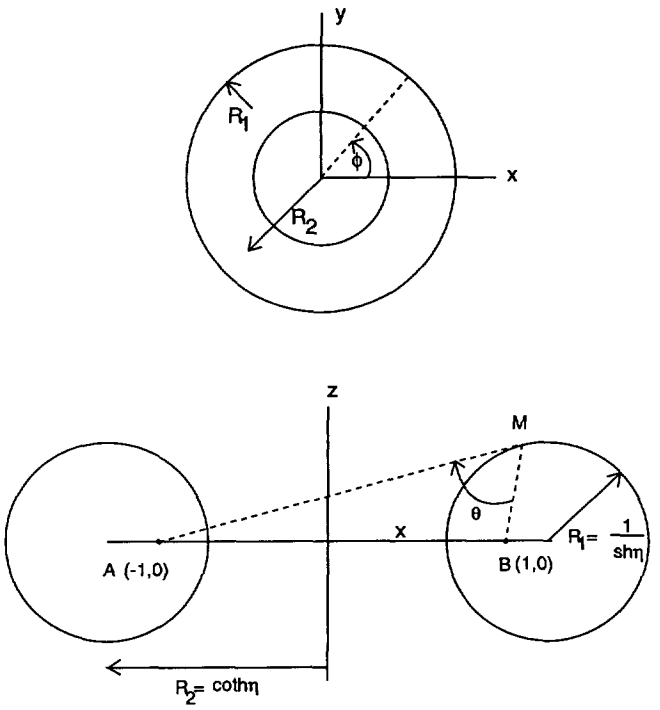

Fig 16. — Toroidal coordinates.

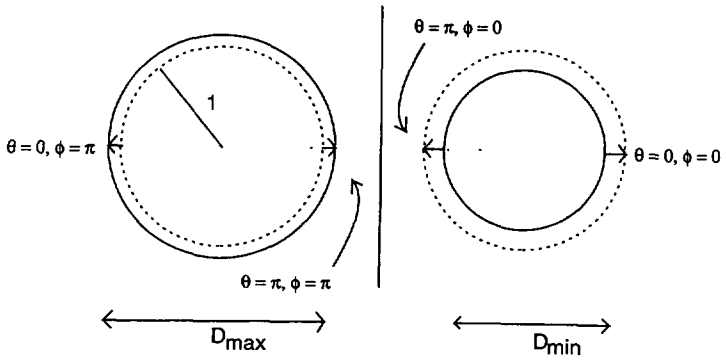

Fig. 17. — Effect of the conformal mode on the Clifford torus. $R_1 = 1$. The unperturbated Clifford torus is represented by dashed circles.

Figure 17 shows the effect of the conformal mode on the Clifford torus. From this, the relative amplitude of the mode reads:

$$a^* = \frac{a}{R_1} = \frac{1}{\sqrt{2}} \frac{D_{max} - D_{min}}{D_{max} + D_{min}}. \tag{A.12}$$

References

[1] Canham P B , *J Theor Biol.* **26** (1970) 61.

[2] Helfrich W., *Z. Naturforsch.* **28c** (1973) 693

[3] Evans E.A., *Biophys. J.* **14** (1974) 923

[4] Lipowsky R., *Nature* **349** (1991) 475.

[5] It can be shown that, to the same order, the curvature elastic energy contains a Gaussian curvature term. $E_G = \bar{\kappa} \oint dS\, C_1 C_2$, where $\bar{\kappa}$ is the Gaussian bending modulus of the membrane However, due to the Gauss-Bonnet theorem, the preceding integral depends only on the topological genus g of the surface: $E_G = \bar{\kappa}(1 - g)$, and thus is of no use in the study of equilibrium shapes of a given genus. For toroidal vesicles, this term simply vanishes

[6] Sheetz M.P. and Singer S.J , *Proc Nat Acad. Sci. U.S.A.* **71** (1974) 4457

[7] Helfrich W., *Z. Naturforsch* **29c** (1974) 510.

[8] Deuling H J. and Helfrich W., *J. Phys. France* **37** (1976) 1335

[9] Bozic B., Svetina S., Zeks B. and Waugh R., *Biophys J* **61** (1992) 963

[10] Waugh R.E., Song J., Svetina S. and Zeks B., *Biophys. J.* **61** (1992) 974.

[11] Miao L., Seifert U., Wortis M. and Döbereiner H G., *Phys. Rev. E* **49** (1994) 5389.

[12] Miao L., Fourcade B , Rao M , Wortis M. and Zia R.K.P., *Phys. Rev. A* **43** (1991) 6843.

[13] Seifert U , Berndl K and Lipowsky R., *Phys. Rev. A* **44** (1991) 1182.

[14] Yager P. and Schoen P.E., *Mol. Cryst. Liq. Cryst* **106** (1984) 371.

[15] Schnur J.M., Price R.R., Schoen P.E., Yager P , Calvert J M., Georger J. and Singh A., *Thin Solid Films* **152** (1987) 181.

[16] Yager P., Price R.R., Schnur J.M., Schoen P.E., Singh A. and Rhodes D.G., *Chem and Phys. of Lipids* **46** (1988) 171.

[17] For axisymmetric vesicles, it is relatively easy to get a "mean" contour of the meridian cross section, by averaging over a few snapshots, in order to get rid of the thermal fluctuations. For almost circular cross sections, an equivalent method is to extract a mean radius averaged over a few snapshots; we used this method. The uncertainty in the calculated reduced volume is related to the uncertainties in the measured radii, and is always less than 5%. For non-circular cross sections, we used a cruder method: among the different snapshots, we retained the one which looked like showing the "average" cross section. The approximation is justified because there was no critical theoretical prediction to test in these cases (such as a precise critical reduced volume). The contour is then modelled by a discrete set of points and approximated by a set of B-spline curves. It is then easy to generate a triangulated model of the whole surface. For nonaxisymmetric vesicles, we again distinguished between almost circular and noncircular cross sections. For almost circular cross sections (i.e., almost Dupin cyclides), we measured the relevant "mean" geometrical parameters as shown in Figure 14 of Appendix 8.4. The uncertainty in the calculated reduced volume is also less than 5%. For non-circular cross sections, we again used a cruder approximation. Starting from a cross section, which we visually estimated as being a good approximation of the "average" side view cross section, we digitized the two corresponding closed curves in the same way as explained above. The triangulated surface approximating the nonaxisymmetric vesicle is then generated using an algorithm, which, applied to the corresponding contour of a Dupin cyclide, leads to this Dupin cyclide This heuristic algorithm is intended to give only an approximation of the observed vesicle. Using the surface evolver program, it is possible to calculate the geometrical parameters $(v, \Delta a)$ of the triangulated surface, and reach the nearest stationary solution of the curvature elastic energy model. Refinement of the triangulation is also possible, in order to get more accurate values of the energy and Lagrange parameters. We checked that the numericallly equilibrated surfaces were stable using a perturbation test available in the program

[18] Brakke K.A., *Experimental Mathematics* **1** (1992) 141.

[19] Mutz M. and Bensimon D., *Phys. Rev. A* **43** (1991) 4525.

[20] Fourcade B., Mutz M. and Bensimon D., *Phys. Rev. Lett.* **68**, 2251 (1992).

[21] Ou-Yang Z.-C., *Phys. Rev. A* **41** (1990) 4517.

[22] Fourcade B., *J. Phys. France* **2** (1992) 1705.

[23] Seifert U., *Phys Rev Lett.* **66** (1991) 2406.

[24] almost circular tori will be called circular tori in the following.

[25] Duplantier B., *Physica A* **168** (1990) 179.

[26] Seifert U., *J. Phys. A: Math. Gen.* **24** (1991) L573.

[27] Jülicher F., Seifert U and Lipowsky R., *J. Phys. II France* **3** (1993) 1681

[28] Strictly speaking and according to JSL, there are only three sheets of stationary shapes: two containing surfaces with up/down symmetry (Di and Si), one containing surfaces with no up/down symmetry (St). The family of almost circular tori (Ci) belongs to the Di sheet.

[29] Such an analysis would have required the precise knowledge of the averaged cross section of the vesicles in the corresponding symmetry planes. Due to the Brownian motion, this was not possible (see below).

[30] Ou-Yang Y.C., *Phys. Rev. E* **47** (1993) 747.

[31] The frequency of the flip-flop phenomenon (a phospholipid molecule suddenly changes its orientation and joins the opposite monolayer) can be measured by spectroscopic means which are sensitive to the headgroup environment These studies have, however, been made only for rather uncontrolled mixtures of phospholipids, mostly for biological membranes which also contain proteins, and the resulting values depend notably on the experimental setup. A typical value for this frequency would be of the order of some hours to some days.

[32] We point out that the observation of such a great relative amplitude of the fluctuations is unique at the moment

[33] Drouffe J.-M. and Fourcade B., private communication. The calculation made by Fourcade in [22] assumes that the meridian and azimutal deformation modes of the Clifford torus are eigenmodes and build a complete set. This second assertion appears to be false: coupled meridian and azimutal modes must be taken into account. However, this change does not give rise to a new zero energy mode: there remains only two zero energy modes to satisfy the geometrical constraints (volume, area and area difference).

[34] Our result is, however, in agreement with the value obtained by Seifert for the *unstable* branch of the discoid family. This branch corresponds to shapes which are unstable with respect to infinitesimal axisymmetry breaking. If one takes into account the Δa constraint (this was not done in Ref. [23]), the shapes might be stable with respect to the subset of axisymmetry-breaking perturbations which keep Δa constant.

[35] The nonprediction of these shapes by JSL is puzzling and might be due to different reasons. First, they performed the stability test with respect to infinitesimal special conformal transformations only, which might be unsufficient to look for very nonaxisymmetric shapes such as the one we observed Secondly, their analysis was limited to the stable shapes of the models, thus skipping all the possible metastable shapes.

[36] Michalet X., Bensimon D. and Fourcade B., *Phys. Rev Lett.* **72** (1994) 168.

[37] Kléman M., *J. Phys. France* **38** (1977) 1511.

[38] Mosseri R , Sadoc J.F. and Charvolin J., in R. Lipowsky, D. Richter, and K. Kremer Eds., The structure and conformation of amphiphilic membranes (Springer-Verlag, 1992) p. 97.